



ELSEVIER

Available online at [www.sciencedirect.com](http://www.sciencedirect.com)**ScienceDirect**

Scripta Materialia 93 (2014) 40–43

[www.elsevier.com/locate/scriptamat](http://www.elsevier.com/locate/scriptamat)

# Thermoelectric properties of an N-type silicon–germanium alloy related to the presence of silica nodules dispersed in the microstructure

Guillaume Bernard-Granger,\* Katia Favier, Mathieu Soulier, Christelle Navone, Mathieu Boidot, Benoit Deniau, Pauline Grondin, Jean Leforestier and Julia Simon

Commissariat à l'Energie Atomique et aux Energies Alternatives, DRT/LITEN/DTNM/SERE/LTE, 17, rue des Martyrs, 38054 Grenoble Cedex 9, France

Received 17 April 2014; revised 12 August 2014; accepted 24 August 2014

Available online 6 September 2014

Tailoring the amount of nanometer-sized nodules made of amorphous silica, resulting from natural oxidation during the processing steps, in an N-type sintered polycrystalline  $\text{Si}_{92}\text{Ge}_{08}$  material is shown as an effective way to reduce the thermal conductivity without affecting significantly the thermoelectric power factor.

© 2014 Acta Materialia Inc. Published by Elsevier Ltd. All rights reserved.

**Keywords:** Thermoelectric materials; Mechanical alloying; Spark plasma sintering; Transmission electron microscopy

The dimensionless figure of merit  $ZT$  ( $Z = S^2\sigma/\lambda$ , where  $S$  is the Seebeck coefficient,  $\sigma$  is the electrical conductivity,  $\lambda$  is the thermal conductivity and  $T$  is the absolute temperature) characterizes the efficiency of a thermoelectric material at a given temperature. The higher the  $ZT$  value, the better the thermoelectric behaviour.

Many approaches to developing compounds for high-temperature applications have been explored for boride-based [1–3] and oxide-based [4] materials. Nonetheless, despite the economic/technological problems to be addressed when mounted in modules (cost of germanium, oxidation in air, diffusion barriers, brazing, etc.), Si–Ge alloys remain an interesting alternative when thermoelectric materials have to operate in the 600–900 °C temperature range [5–7].

A strong improvement in  $ZT$  (in comparison with standard several-micrometer-sized SiGe materials used in radioisotope thermoelectric generators (RTGs) for space missions) is observed when fully dense N-type (majority carriers are electrons,  $ZT$  of 1.3 at 800 °C, 53% improvement) and P-type  $\text{Si}_{80}\text{Ge}_{20}$  (majority carriers are holes,  $ZT$  of 1 at 800 °C, 100% improvement) bulk polycrystals with a nanometer grain size ( $\sim 20$  nm for both materials) are manufactured [8,9]. These results are in agreement with theoretical calculations showing that nanostructuring well-known thermoelectric materials enables  $ZT$  values much higher than 1 to be achieved [10,11]. Nonetheless, such bulk nanostructured materials may have drawbacks when

exposed to high temperatures (grain growth modifying the thermoelectric properties under service conditions, irreversible deformation and/or rupture of the thermoelements made of such materials if service conditions enable creeping by grain boundary sliding at medium temperatures under moderate applied stresses, etc.), as could be the case for thermoelectrical applications.

Recently, it has also been shown that dispersing 1.3 vol.%  $\text{MoSi}_2$  nanometer-size inclusions homogeneously in an N-type  $\text{Si}_{92}\text{Ge}_{08}$  polycrystalline matrix (average grain size  $\sim 1$   $\mu\text{m}$ ) leads to a material having a  $ZT$  of  $\sim 1.0$  at 700 °C [12]. This value has to be compared to 0.7, at the same temperature, for a sintered material made from the matrix alone [12]. In the composite and matrix materials investigated it was also shown that a small fraction of native silica nodules ( $\sim 4.5\text{--}4.7 \times 10^{-5}$  nodule/ $\text{nm}^2$ , due to natural oxidation that occurs during the different processing steps used to manufacture the polycrystals), having an average diameter of  $\sim 60\text{--}70$  nm, was homogeneously dispersed in the as-sintered microstructures [12]. We may wonder about the influence of such nodules alone on the thermoelectrical properties of the materials investigated. Consequently, in this paper we report the influence of nanometer-size native silica nodules on the thermoelectrical properties of an N-type polycrystalline  $\text{Si}_{92}\text{Ge}_{08}$  alloy.

Two granulated N-type  $\text{Si}_{0.913}\text{Ge}_{0.080}\text{P}_{0.007}$  compositions (phosphorous belongs to group V of the periodic table whereas silicon and germanium belong to group IV: extra valence electrons are added that become unbonded from individual atoms and allow the compound to be an electrically conductive N-type semiconductor) were produced by

\* Corresponding author; e-mail: [guillaume.bernard-granger@cea.fr](mailto:guillaume.bernard-granger@cea.fr)

**Table 1.** Purity, shape and size of the silicon, germanium and phosphorous precursors used to produce the powders of interest.

Element	Si	Ge	P
Purity (%)	99.99	99.999	99.999
Shape	Powder	Chunks	Chunks
Size ( $\mu\text{m}$ )	40	3000/6000	100
			3000/6000
			100

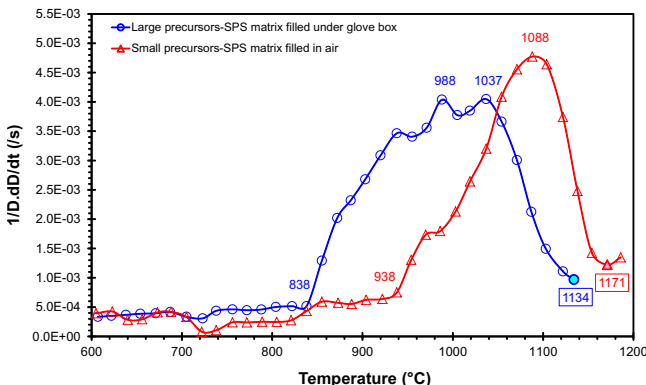
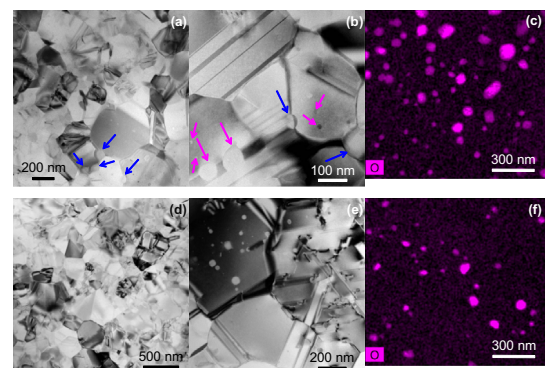
mechanical alloying, in an argon atmosphere using tailored experimental conditions [12]. The first composition, named “Large precursors” or “LP”, is prepared from silicon and germanium chunks (Neyco, see purities and size in Table 1). The second one, named “Small precursors” or “SP”, is prepared from silicon and germanium powders (Neyco, see purities and size in Table 1). In both cases, the same phosphorous precursor (Neyco, powder, 99.5%, 100  $\mu\text{m}$ ) is incorporated. All the precursors were delivered under argon by the supplier. As observed previously [12], both collected powders are made of aggregates having diameters in the range 2–20  $\mu\text{m}$  and each aggregate is composed of elemental crystallites having an average diameter of  $\sim 20$  nm (determined by the Williamson–Hall method from X-ray diffraction patterns [12,13]).

Spark plasma sintering (SPS) has proved to be an efficient method to sinter semiconductor powders in a short time, with perfect control of the final microstructure [12,14–15]. For both powders of interest, SPS runs were conducted in vacuum, using an HPD-25 sintering setup (FCT Systeme GmbH). Experimental conditions are described in a previous paper [12]. Nonetheless, it is important to point out that, for the “LP” powder, filling of the die was completed in a glovebox, under an argon atmosphere. For the “SP” powder, filling was done simply in ambient air.

For the powders investigated, the evolution of the densification rate as a function of temperature is shown in Figure 1. In both cases a typical bell-shape curve is observed, as usually the case for semiconductor powders [12,14,15]. For both powders, we selected soak temperatures at the bottom of the bell-shape curves at which point densification is complete. Consequently, with all other parameters fixed [12], two samples were sintered with a 5 min soak time at 1130 and 1170 °C for the “LP” and “SP” powders, respectively. After soaking, the samples were cooled naturally by shutting-down the SPS equipment. The apparent density of as-sintered samples was measured using the Archimedes method with deionized water. The final relative density,  $D_f$ , was obtained using a theoretical density of

2.598 g  $\text{cm}^{-3}$ . Both as-sintered samples have a relative density of 99%. Their oxygen content was measured (thermal decomposition, LECO CS300). Concentrations of 4.4 and 0.6 at.% were obtained for the samples sintered from the “SP” and “LP” powders, respectively. It is then postulated that the raw powder processed from “SP” oxidizes significantly during the filling step of the SPS matrix performed in ambient air. However, such an oxidation phenomenon is limited (not completely removed) when the raw powder processed from “LP” is introduced into the SPS matrix in a glovebox filled with argon. The difference in oxygen content between both powders investigated may explain why they exhibit different densification behaviors, as reported in Figure 1, even though they have the same elemental crystallite size.

The microstructures of the as-sintered samples were investigated in depth. Thin foils were prepared from the central zone of each sintered pellet and observed by transmission electron microscopy (TEM) using a Tecnai Osiris microscope (FEI, acceleration voltage of 200 kV, point-to-point resolution of 2.5 Å) equipped with a high-angle annular dark-field detector (HAADF) and an energy-dispersive spectroscopy (EDS) microanalysis system. Figure 2a,b and d,e show the typical microstructure observed by TEM in the as-sintered samples made from the “SP” and “LP” powders, respectively. Both samples exhibit very similar microstructures. They are fully dense polycrystals, in agreement with their relative densities measured to be 99%. The individual grains have a polygonal shape. Most of them appear twinned when they are tilted under the electron beam. Figure 3a shows that the grain size distribution is similar for both samples (the method used to determine the grains size is detailed in a previous paper [12]). A similar average grain size of  $\sim 410$  nm is measured. The average composition of the individual grains determined from EDS analyses is  $90.93 \pm 0.40$  at.% Si,  $8.66 \pm 0.39$  at.% Ge,  $0.41 \pm 0.10$  at.% P for the material made from the “LP” powder vs.  $90.86 \pm 0.26$  at.% Si,  $8.63 \pm 0.24$  at.% Ge,  $0.52 \pm 0.08$  at.% P for the material sintered from the “SP” powder. Whatever the sample observed, it should be

**Figure 1.** Evolution of the densification rate as a function of temperature for the “LP” and “SP” powders.**Figure 2.** Typical microstructures and oxygen EDS maps acquired on the as-sintered samples made from the “SP” and “LP” powders.

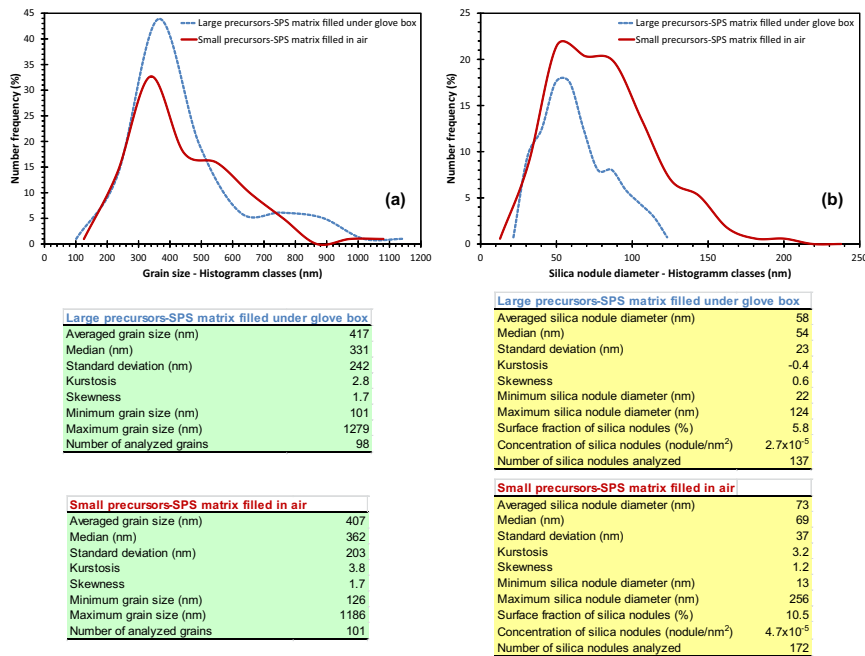


**Figure 3.** (a) Grain size distribution and associated statistics collected from the microstructure analyses performed on as-sintered samples made from the “LP” and “SP” powders. (b) Silica nodule diameter distribution and associated statistics collected from the microstructure analyses performed on as-sintered samples made from the “LP” and “SP” powders.

noted that phosphorous EDS maps show that a significant amount of this element is segregated at grain boundaries. Spherical nodules of a second phase are distributed in both as-sintered microstructures where they can have intragranular (pink arrows on Fig. 2b and all nodules on Fig. 2e) and intergranular positions (blue arrows on Fig. 2a and b). Based on high-resolution TEM mode and EDS analyses, it is concluded that these nodules are made of amorphous silica, whatever the sample observed. Finally, the only difference between the as-sintered microstructures is in the amount/size of amorphous silica nodules that are observed. Oxygen EDS maps show that the volume fraction of silica nodules is higher for the material sintered from the “SP” powder (Fig. 2c) in comparison to the one sintered from the “LP” powder (Fig. 2f). Figure 3b confirms this point. The concentration of amorphous silica nodules is

$\sim 2.7 \times 10^{-5}$  nodule/nm<sup>2</sup> for the sample sintered from the “LP” powder vs.  $4.7 \times 10^{-5}$  nodule/nm<sup>2</sup> (74% higher) for the one sintered from the “SP” powder. If for both samples the average nodule diameter is in the range 60–70 nm, it should be noted that the nodule distribution size is larger for the sample made from the “SP” powder (the method used to determine the nodule diameters is detailed in a previous paper [12]). Consequently, the material sintered from the “SP” powder is clearly more oxidized than the one made from the “LP” powder. The consequence of such an oxidation phenomenon is the presence of a certain amount (proportional to the oxidation efficiency) of native amorphous silica nodules that are homogeneously dispersed in the sintered microstructures.

The electrical conductivity and Seebeck coefficient evolutions as function of temperature (ZEM-3, Ulvac GmbH,

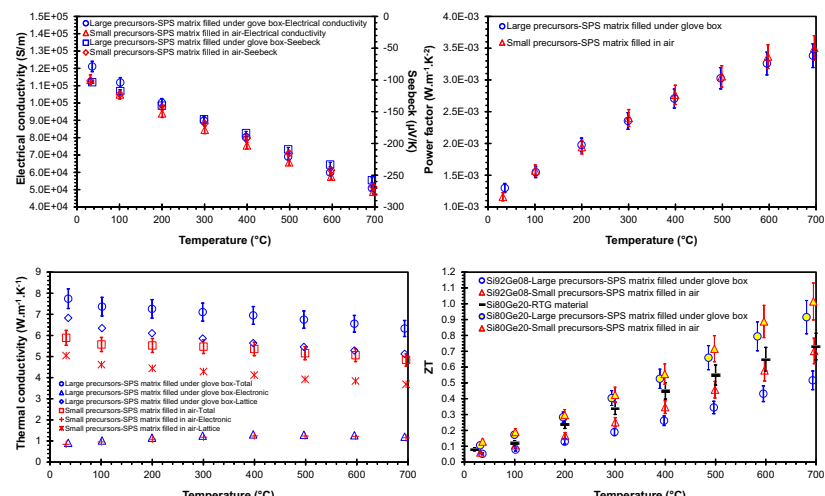


**Figure 4.** Thermoelectrical properties as a function of temperature measured on the as-sintered samples made from the “LP” and “SP” powders: (a) electrical conductivity and Seebeck coefficient; (b) power factor; (c) thermal conductivity including the electronic and lattice contributions; (d) ZT parameter.

helium working atmosphere, overall measurement errors are  $\pm 2.5\%$  and  $\pm 1.5\%$  for electrical conductivity and Seebeck coefficient, respectively) for both as-sintered samples are shown in Figure 4a. There is no significant difference between both samples. Consequently, the evolutions of the power factor ( $\sigma S^2$ ) as a function of temperature are also similar (Fig. 4b). The carrier concentrations and their mobility at room temperature for both as-sintered materials have been measured (Hall effect, HMS-3000, Four Point Probes/Bridge Technology, Chandler Heights, ambient working atmosphere). Whatever the sample measured, the carrier concentration is in the range  $1.7\text{--}1.9 \times 10^{20}$  carriers  $\text{cm}^{-3}$  and the mobility is in the range  $33\text{--}36 \text{ cm}^2 \text{ V}^{-1} \text{ s}^{-1}$ .

Figure 4c shows the evolution of the thermal conductivity as a function of temperature for both as-sintered materials. The thermal conductivity,  $\lambda$ , is calculated as the product of the thermal diffusivity (laser flash method, LFA 457 MicroFlash®, Netzsch-Gerätebau GmbH, argon working atmosphere), the specific heat (differential scanning calorimetry, DSC 404 F1 Pegasus, Netzsch-Gerätebau GmbH, argon working atmosphere) and the mass density of the samples (the overall measurement error is  $\pm 6\%$ ). The total conductivity of the as-sintered material made from the “SP” powder is significantly lower than that of the as-sintered sample made from the “LP” powder. Looking at the electronic and lattice contributions is also very important (we estimated the carrier part via the Wiedemann–Franz–Lorenz relation:  $\lambda_e = L_0 T \sigma$ , with a Lorenz number  $L_0$  of  $2.45 \times 10^{-8} \text{ V}^2 \text{ K}^{-2}$  that applies for degenerate semiconductors. The lattice thermal conductivity  $\lambda_l$  is then deduced from the simple relation  $\lambda = \lambda_e + \lambda_l$ ). The electronic part of the thermal conductivity is similar for both samples. However, the lattice part of the thermal conductivity is much lower for the as-sintered sample made from the “SP” powder in comparison to that of the as-sintered sample made from the “LP” powder. Consequently, the decrease in lattice-thermal conductivity for the sample sintered from the “SP” powder, in comparison to the one of the material made from the “LP” powder, is probably related to the higher concentration of silica nodules. Such nodules, homogeneously dispersed in the microstructure, are thought to perturb lattice vibrations, lowering the thermal diffusivity and then directly the thermal conductivity, without affecting the power factor. For a  $\text{Si}_{1-x}\text{Ge}_x$  system, the mean free paths for electrons and phonons are in the range 2–5 and 2–300 nm, respectively, for heavily doped materials at room temperature [5]. Consequently, the silica nodules distributed in the microstructure of the sintered samples we investigated are able to perturb lattice vibrations but are too large to interact with the electron path. Hence, the higher concentration of silica nodules in the as-sintered material made from the “SP” powder explains why the thermal conductivity is lower than that of the material made from the “LP” one. For the same reason,

the electrical conductivities of both materials are similar, as are the power factors.

The dimensionless figure of merit as a function of temperature for both as-sintered materials is shown in Figure 4d. Irrespective of the temperature, the sample made from the “SP” powder has a higher ZT than that of the sample made from the “LP” powder. The sample made from the “SP” powder is also not too far from N-type  $\text{Si}_{80}\text{Ge}_{20}$  RTG materials, the advantage of the materials we investigated being the lower amount of germanium used (germanium is expensive, around \$1250 per kg for 99.99% purity and one metric ton of material).

Therefore, tailoring the concentration of native nanometer-sized amorphous silica inclusions could be a way to reduce significantly the lattice contribution to the thermal conductivity of as-sintered N-type  $\text{Si}_{92}\text{Ge}_{8}$  polycrystalline materials, without affecting significantly the power factor. This strategy has been also successfully applied to an N-type  $\text{Si}_{80}\text{Ge}_{20}$  as-sintered polycrystalline material (Fig. 4d).

The research leading to these results has received funding from the Seventh Framework Program (FP7/2007–2013) under Grant Agreement No. 263440 (NEAT project). We also thank the Hot Block OnBoard company (Grenoble) for their support.

- [1] C. Wood, D. Emin, Phys. Rev. B 29 (1984) 4582.
- [2] T. Mori, T. Nishimura, J. Solid State Chem. 179 (2006) 2908.
- [3] S. Maruyama, Y. Miyazaki, K. Hayashi, T. Kajitani, T. Mori, Appl. Phys. Lett. 101 (2012) 152101.
- [4] I. Terasaki, in: K. Koumoto, T. Mori (Eds.), “Thermoelectrics Nanomaterials”, Springer Series in Materials Science, 182, Springer Verlag, Berlin, 2013, pp. 51–70.
- [5] Y. Lan, A.J. Minich, G. Chen, Z.F. Ren, Adv. Funct. Mater. 20 (2010) 357.
- [6] A.J. Minich, M.S. Dresselhauss, Z.F. Ren, G. Chen, Energy Environ. Sci. 2 (2009) 466.
- [7] C.J. Vineis, A. Shakouri, A. Majumdar, M.G. Kanatzidis, Adv. Mater. 22 (2010) 3980.
- [8] G. Joshi, H. Lee, Y. Lan, X. Wang, G. Zhu, D. Wang, R.W. Gould, D.C. Cuff, M.Y. Tang, M.S. Dresselhaus, G. Chen, Z. Ren, Nano Lett. 8 (2008) 4670.
- [9] X.W. Wang, H. Lee, Y.C. Lan, G.H. Zhu, G. Joshi, D.Z. Wang, J. Yang, A.J. Muto, M.Y. Tang, J. Klatsky, D. Song, M.S. Dresselhaus, G. Chen, Z.F. Ren, Appl. Phys. Lett. 93 (2008) 193121.
- [10] L.D. Hicks, M.S. Dresselhaus, Phys. Rev. B 47 (1993) 16631.
- [11] L.D. Hicks, M.S. Dresselhaus, Phys. Rev. B 47 (1993) 12727.
- [12] K. Favier, G. Bernard-Granger, C. Navone, M. Soulier, H. Boidot, J. Leforestier, J. Simon, J.-C. Tedenac, D. Ravot, Acta Mater. 64 (2014) 429.
- [13] G.K. Williamson, W. Hall, Acta Metall. 1 (1953) 22.
- [14] G. Bernard-Granger, A. Néri, C. Navone, M. Soulier, J. Simon, Marinova-Atanassova, J. Mater. Sci. 47 (2012) 4313.
- [15] R. Vrancar, G. Bernard-Granger, C. Navone, M. Soulier, M. Boidot, J. Leforestier, J. Simon, J. Alloys. Compd. 598 (2014) 272.